batteries

MDPI

Article

Study on Blended Terpolymer Electrolyte Membrane for Enhanced Safety and Performance in Lithium-Ion Batteries

Wansu Bae, Sabuj Chandra Sutradhar, Subeen Song, Kijong Joo, Doyul Lee, Donghoon Kang, Hyewon Na, Jiye Lee, Whangi Kim and Hohyoun Jang *

Department of Energy Material Science, Konkuk University, 268 Chungwon-daero, Chungju 27478, Republic of Korea; gelp621@naver.com (W.B.); chandra@kku.ac.kr (S.C.S.); hubsugar@naver.com (S.S.); joo10140@naver.com (K.J.); b6769@naver.com (D.L.); rkdehdgns28@naver.com (D.K.); gpdnjs3z3@naver.com (H.N.); wldp9902@naver.com (J.L.); wgkim@kku.ac.kr (W.K.)
* Correspondence: 200417450@kku.ac.kr

Abstract: The persistent emphasis on safety issues in lithium-ion batteries (LIBs) with organic liquid electrolytes revolves around thermal runaway and dendrite formation. The high thermal stability and non-leakage properties of polymer electrolytes (PEs) make them attractive as next-generation electrolytes for LIBs. This study presents a blended terpolymer electrolyte (BTPE) membrane, integrating the high ionic conductivity of dual ion conducting polymer electrolytes (DICPEs) with the elevated lithium transference number (t_+) of single-ion conducting polymer electrolytes (SICPEs). The BTPE was synthesized by blending PAA–PVA with lithiated acrylic acid (LiAA), lithiated 2–acrylamido–2–methylpropane sulfonic acid (LiAMPS), and a 2–hydroxyethyl methacrylate (HEMA)–based terpolymer, using lithium bis(fluorosulfonyl)imide (LiFSI) as the lithium salt. The synthesized BTPE showed excellent physical and electrochemical stability; it also exhibited an enhanced lithium transference number (t_+ = 0.47) and high ionic conductivity (5.21×10^{-4} S cm^{-1} at 30 °C), attributed to the interaction between the FSI anion and the NH group of AMPS. This research presents an innovative strategy for the design of next-generation LIB electrolytes by integrating polymer electrolytes.

Keywords: polymer; polymer electrolyte; lithium metal batteries

Academic Editors: Leon L. Shaw and Maziar Ashuri

Received: 23 February 2025
Revised: 8 March 2025
Accepted: 9 March 2025
Published: 11 March 2025

Citation: Bae, W.; Sutradhar, S.C.; Song, S.; Joo, K.; Lee, D.; Kang, D.; Na, H.; Lee, J.; Kim, W.; Jang, H. Study on Blended Terpolymer Electrolyte Membrane for Enhanced Safety and Performance in Lithium-Ion Batteries. *Batteries* **2025**, *11*, 103. https://doi.org/10.3390/batteries11030103

1. Introduction

Currently, lithium-ion batteries (LIBs) are widely used in electric vehicles, portable devices, and energy storage systems (ESS) because of their high energy density and excellent charge–discharge performance [1]. These LIBs play an important role in solving the problem of environmentally friendly energy shortages by reducing environmental pollution and fossil fuel dependence [2,3]. Despite their advantages, such as high ionic conductivity, easy manufacturing, and low interfacial resistance, commercial organic liquid electrolytes in LIBs have notable limitations. Notable issues include the thermal runaway phenomenon at high temperatures and the explosions caused by electrolyte leakage from external impacts [4–7]. Additionally, lithium dendrites, which form during the charge–discharge process, can cause internal short circuits and ignite the solvent through direct contact with electrodes. Despite the development of numerous additives for organic liquid electrolytes to counter these drawbacks, the fire risk remains [8–16]. To overcome these problems, research is increasingly focusing on polymer electrolytes (PEs) which are standing out as promising options. The solid-state nature of PEs ensures higher safety than liquid electrolytes by preventing leakage and inhibiting dendrite growth [17–20]. Among polymer electrolytes,

solid-state polymer electrolytes (SPEs) and gel polymer electrolytes (GPEs) derived from poly (ethylene oxide) (PEO) have received the most research attention. SPEs are prepared by incorporating lithium salts into a polymer matrix [21–24], while GPEs enhance the mobility of lithium ions by adding solvents to the polymer [25–27]. Dual-ion conducting polymer electrolytes (DICPEs), which combine polymers and lithium salts, achieve high ion conductivity due to the mobility of both cations and anions of the lithium salt. However, they exhibit low lithium transference numbers (t_+) because of anion movement [28–30]. A low lithium transference number (t_+) causes concentration polarization, resulting in lithium dendrite formation which remains an unsolved issue [31,32].

To address the low Li^+ ion transference numbers in polymer electrolytes, single-ion conducting polymer electrolytes (SICPEs) have been developed. SICPEs achieve high lithium transference numbers (t_+) by chemically binding the anion to the polymer backbone, thereby allowing only lithium cations to move [20,33,34]. Liew et al. fabricated a nanocomposite polymer electrolyte membrane (NCPEM) based on poly (acrylic acid) and TiO_2 using a solution casting technique, achieving a high ionic conductivity of 8.36×10^{-4} S cm^{-1} and electrochemical stability [35]. Gao et al. reported an electrolyte for Li–S batteries based on SiO_2–g–PAMPSLi@PEO, which maintained a stable discharge capacity of 875.2 mAh g^{-1} after 200 cycles [36]. Hu et al. developed PAS/PS using PVDF–HFP–g–AMPSLi, SiO_2, and PEO, which demonstrated a lithium transference number (t_+) of 0.96 and an ionic conductivity of 5.4×10^{-5} S cm^{-1} at 60 °C [37]. Although SICPEs exhibit excellent electrochemical stability and high lithium transference numbers (t_+), they still suffer from low ionic conductivity (10^{-5}~10^{-7} S cm^{-1} at 25 °C) and require improvement.

This study aims to develop a polymer electrolyte that combines the advantages of SICPE and DICPE. To address this, we prepared a terpolymer based on lithiated acrylic acid (LiAA), lithiated 2–acrylamido–2–methylpropane sulfonic acid (LiAMPS), and 2–hydroxyethyl methacrylate (HEMA), blended it with PAA–PVA, and added LiFSI as a lithium salt to design an ion-conductive blended terpolymer electrolyte membrane (BTPE). LiAMPS and LiAA as Lewis bases, effectively release Li^+ ions, ensuring high ion conductivity [38]. Additionally, AMPS increases the Li^+ transference number by fixing FSI anions through hydrogen bonding between the NH groups and the fluorine (F) atoms of FSI anions [39]. HEMA was polymerized to improve the flexibility of the polymer electrolyte membrane [40], while PVA–PAA increased the mechanical strength and facilitated Li^+ ions' movement through coordination with the unshared electron pair of oxygen atoms [41,42]. The effects of the electrochemical, structural, and thermal properties of the manufactured BTPE were reported. The ionic conductivity and electrochemical properties of BTPE were assessed using electrochemical impedance spectroscopy (EIS), linear sweep voltammetry (LSV), cyclic voltammetry (CV), chronoamperometry (CA), and charge–discharge battery testing. The structural properties of BTPE were examined by using nuclear magnetic resonance (NMR), Fourier transform infrared (FT–IR) spectroscopy, and atomic force microscopy (AFM). The thermal properties of BTPE were analyzed using differential scanning calorimetry (DSC) and thermogravimetric analysis (TGA).

2. Experimental

2.1. Materials

Acrylic acid (AA, >96%), 2–Acrylamido–2–methylpropane sulfonic acid (AMPS, powder) and 2–Hydroxyethyl methacrylate (HEMA, >96%) were obtained from Sigma–Aldrich (Seoul, Republic of Korea). Lithium bis(fluorosulfonyl)imide (LiFSI, high purity, >99.9%), Lithium hydroxide (LiOH), and Ammonium persulfate (APS) were also sourced from Sigma–Aldrich (Seoul, Republic of Korea). Poly (acrylic acid)–poly (vinyl alcohol) (PAA–PVA) was provided by EPchemtech (Gunsan, Republic of Korea). Solvents such as di-

ethyl carbonate (DEC, ≥99%, H_2O < 10 ppm, acid <10 ppm), ethylene carbonate (EC ≥ 99%, H_2O < 10 ppm, acid <10 ppm), and N–methyl–2–pyrrolidone (NMP) were ordered from Sigma–Aldrich (Seoul, Republic of Korea). Lithium iron (II) phosphate ($LiFePO_4$), Poly (vinylidene fluoride) (PVDF) and carbon black (super P, Timcal) were purchased from Alfa Aesar (Seoul, Republic of Korea). 2032 Coin cell kits, aluminum foil, and lithium foil (0.25 mm) were acquired from MTI Corporation (Richmond, CA, USA).

2.2. Synthesis of Poly (LiAA-HEMA-LiAMPS)

All polymer electrolyte films were fabricated using solution casting technology. To prepare the polymer solution, 1.33 g of acrylic acid (AA, 0.0185 mol) and 4.78 g of 2–acrylamido–2–methylpropane sulfonic acid (AMPS, 0.0231 mol) was dissolved in 70 mL of deionized water. Once AA and AMPS were completely dissolved, 1 equivalent of LiOH (0.0415 mol) was added and the mixture was stirred at 40 °C for 2 h to achieve lithiation. Lithiation completion was confirmed using a pH meter. Subsequently, 0.6 g (0.00461 mol) of 2–hydroxyethyl methacrylate (HEMA) was added and stirred for 30 min. Finally, 0.2 g of ammonium persulfate (APS) dissolved in 5.70 mL of deionized water was added to the solution and stirred for 24 h at 70 °C to synthesize the poly (LiAA–HEMA–LiAMPS) solution. The molar ratio of AA, AMPS, and HEMA used was 4:5:1 (Scheme 1).

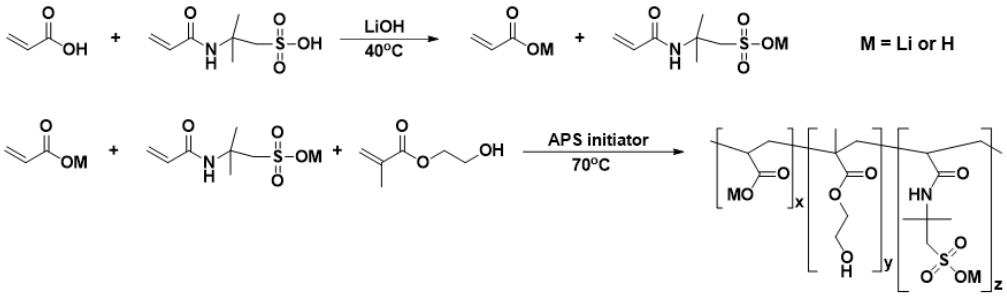

Scheme 1. Synthesis of the terpolymer poly (LiAA-HEMA-LiAMPS).

2.3. Preparation of Blended Terpolymer Electrolyte

The synthesized terpolymer solution was mixed with a 3% aqueous solution of PAA–PVA, serving as a plasticizer, at various polymer weight ratios. The mixture was stirred for 1 h. Subsequently, the lithium bis(fluorosulfonyl)imide (LiFSI) was added and the solution was stirred for an additional 30 min. The resulting mixture was then poured into a silicon mold, placed on glass and dried in an oven at 40 °C for 24 h to form the mixed terpolymer electrolyte membrane. As the ratio of terpolymer increased, the phase separation of terpolymer and PAA–PVA occurred, preventing the formation of a uniform surface (as shown in Figure S1). Therefore, the blended terpolymer electrolyte (BTPE) used in the experiment was prepared according to specifications in Table 1.

Table 1. Composition and ratio of blended terpolymer electrolyte membrane.

Electrolyte Name	Weight of Pure Terpolymer (g)	Wight of Pure PAA–PVA (g)	Ratio	Weight of LiFSI (g)
BTPE–010 2M	0	0.5	0:10	0.187
BTPE–19 2M	0.05	0.45	1:9	0.187
BTPE–28 2M	0.1	0.4	2:8	0.187
BTPE–37 2M	0.15	0.35	3:7	0.187

2.4. Preparation of LFP Cathode

Lithium ferrous phosphate (LFP), super P, and PVDF were mixed in a ratio of 8:1:1 and dissolved in N–Methyl–2–pyrrolidone (NMP). The resulting cathode slurry was prepared

using a ball mill. This slurry was then cast on Al foil using a doctor blade coater. The coated foil was dried in an oven at 100 °C for 12 h, followed by drying in a vacuum oven at 100 °C for 12 h. The final LFP cathode was obtained by punching 13 mm discs under an argon atmosphere.

2.5. Cell Assemblies

Cell A (SS/BTPE/SS): To measure the ionic conductivity of the polymer electrolytes, a blended terpolymer electrolyte was wetted with ethylene carbonate (EC) and diethyl carbonate (DEC) solvents in a 1:1 weight ratio. The wetted electrolyte was then sandwiched between stainless steel and sealed in a 2032 coin cell to form a symmetrical cell.

Cell B (Li/BTPE/Li): A symmetric cell was fabricated by sandwiching a blended terpolymer electrolyte, soaked in EC and DEC (weight ratio 1:1) solvents, between two Li foils (16 mm). This assembly was then sealed in a 2032 coin cell. The resulting Li symmetric cell was used to measure the ion transfer number of the polymer electrolyte.

Cell C (SS/BTPE/Li): To measure the linear sweep voltage (LSV) of the polymer electrolytes, blended terpolymer electrolytes were wetted with EC and DEC (weight ratio 1:1) solvents. These electrolytes were then sandwiched between stainless steel and Li foil and sealed in a 2032 coin cell to create an asymmetric cell.

Cell D (LFP/BTPE/Li): A polymer electrolyte membrane, soaked in EC/DEC (weight ratio 1:1) solvents, was placed between a Li metal foil and an LFP cathode. This assembly was then sealed in a 2032 cell. The fabricated Li metal cell was subsequently used for battery testing.

2.6. The Structural Characterization of the Polymer Electrolytes

The chemical structure of the lithium-substituted monomer and polymer was identified using ^{1}H–NMR on an Avance 400FT–NMR 400 MHz (Bruker, Billerica, MA, USA), with D_2O and DMSO–d_6 as the solvent. Fourier transform infrared spectroscopy (FT–IR) was employed to measure the structures of the precursor and the synthesized terpolymer electrolytes (TPE) using a Nicolet Summit (Thermo Fisher Scientific, Waltham, MA, USA) over a scan range of 4000 to 500 cm^{-1} with a resolution of 4 cm^{-1}. The surface topography and phase separation morphology of the blended terpolymer and PAA–PVA films were recorded using an atomic force microscope (AFM) utilizing an FX40 (Parksystems, Suwon, Republic of Korea) at room temperature. AFM images were obtained in tapping mode with an aluminum-coated cantilever capturing at various locations.

2.7. Thermal Performance Test

Thermogravimetric analysis (TGA) was conducted to evaluate the thermal stability of the terpolymer electrolytes using a TGA–N1000 analyzer (Scinco, Seoul, Republic of Korea). The analysis was performed over a temperature range of room temperature (RT) to 800 °C at a heating rate of 10 °C min^{-1} under an inert nitrogen (N_2) atmosphere. Differential scanning calorimetry (DSC) was used to determine the glass transition temperature (T_g) of the electrolytes. Measurements were taken using a DSC 6000 (Perkin Elmer, Waltham, MA, USA) between −60 to 200 °C at a heating rate of 10 °C min^{-1} under a N_2 flow environment.

2.8. Electrochemical Measurements

Electrochemical impedance spectroscopy (EIS) was utilized to measure for ion conductivity of the BTPEs using an IM6ex (Zahner–Elektrik, Kronach, Germany). Measurements were taken between room temperature and 80 °C, across a frequency range of 1 MHz to

10 Hz with an alternating current (AC) amplitude of 10 mV. The ionic conductivity of the BTPE was calculated using the following Equation (1):

$$\sigma = \frac{l}{RA} \tag{1}$$

where, σ (S cm^{-1}) is the ionic conductivity, and l (cm) and A (cm^2) represent the thickness and the area of the terpolymer electrolyte membrane, respectively. R is the bulk interfacial resistance (Ω) of the polymer electrolyte.

The lithium-ion transference number (t_+) of the terpolymer electrolyte was obtained from the chronoamperometry (CA) and electrochemical impedance spectroscopy (EIS) data, both before and after CA measurements. The CA test was conducted at a voltage of 1 mV for 10,000 s. EIS measurements were performed over a frequency range of 1 MHz to 10 Hz with an amplitude of 10 mV. The lithium-ion transference number (t_+) of the electrolyte was calculated using the following Equation (2), based on the Bruce–Vincent method:

$$t_+ = \frac{I_s(\Delta V - I_0 R_0)}{I_0(\Delta V - I_s R_s)} \tag{2}$$

where t_+ is the lithium-ion transference number, I_0 and I_s represent the initial and steady-state currents, ΔV is the constant applied DC voltage of the cell, and R_0 and R_s are the initial and steady-state interfacial resistances of the polymer electrolyte, respectively.

The linear scanning voltammetry of BTPE and the cyclic voltammetry (CV) of the lithium-ion battery were measured over a voltage range of –1.5 to 6 V (vs. Li/Li^+) at the scanning rate of 1 mV s^{-1}. CA, LSV, and CV measurements were conducted using Squidstat plus (Admiral instruments, Tempe, AZ, USA).

The battery test was performed by cycling the cells from 2.5 to 3.8 V (vs. Li/Li^+) at different C rates at 40 °C using the battery tester CT4008T (Neware, Shenzhen, China).

3. Results and Discussions

3.1. Characterization of Poly (LiAA-HEMA-LiAMPS) Terpolymer

Figure 1 represents the ^{1}H NMR spectra of HEMA, LiAA, LiAMPS, and poly (LiAA–HEMA–LiAMPS). In Figure 1a, peaks at 6.05 ppm and 5.65 ppm correspond to the ethylene group protons (‘a’), and the peak at 1.89 ppm corresponds to the protons (‘b’). The peaks at 4.15 ppm and 3.73 ppm correspond to protons (‘c’) and (‘d’) [43]. Figure 1b shows peaks at 6.02 ppm and 5.87 ppm for the ethylene group protons of AA (‘a’), and the peak at 5.32 ppm for the C=CH_2 proton (‘b’). Small peaks around 6.13, 5.90, and 4.24 ppm indicate the presence of AA without lithium substitution. In Figure 1c, the proton peak of C=CH_2 (‘a’) appears at 6.00 ppm, and the peak of C=CH– (‘b’) appears at 5.50 ppm. In addition, the peak at 8.33 ppm corresponds to the –NH proton (‘c’), and peaks at 1.38 ppm and 2.69 ppm correspond to –CH_3 (‘d’) and protons (‘e’), respectively [44]. Figure 1d shows the ^{1}H NMR spectrum of synthesized poly (LiAA–HEMA–LiAMPS) with peaks at 1.39 ppm for –CH_2– protons in the polymer backbone (‘a, a1, a2’), and –CH_3 protons (‘d’ and ‘f’), at 1.98 ppm for –CH– protons (‘b, b1’), at 7.51 ppm for –NH protons (‘c’), and at 3.29, 3.70, and 4.12 ppm for –CH_2– protons (‘e’, ‘h’, and ‘g’). This characterization confirms the successful synthesis of the poly (LiAA–HEMA–LiAMPS) terpolymer with the expected chemical structure.

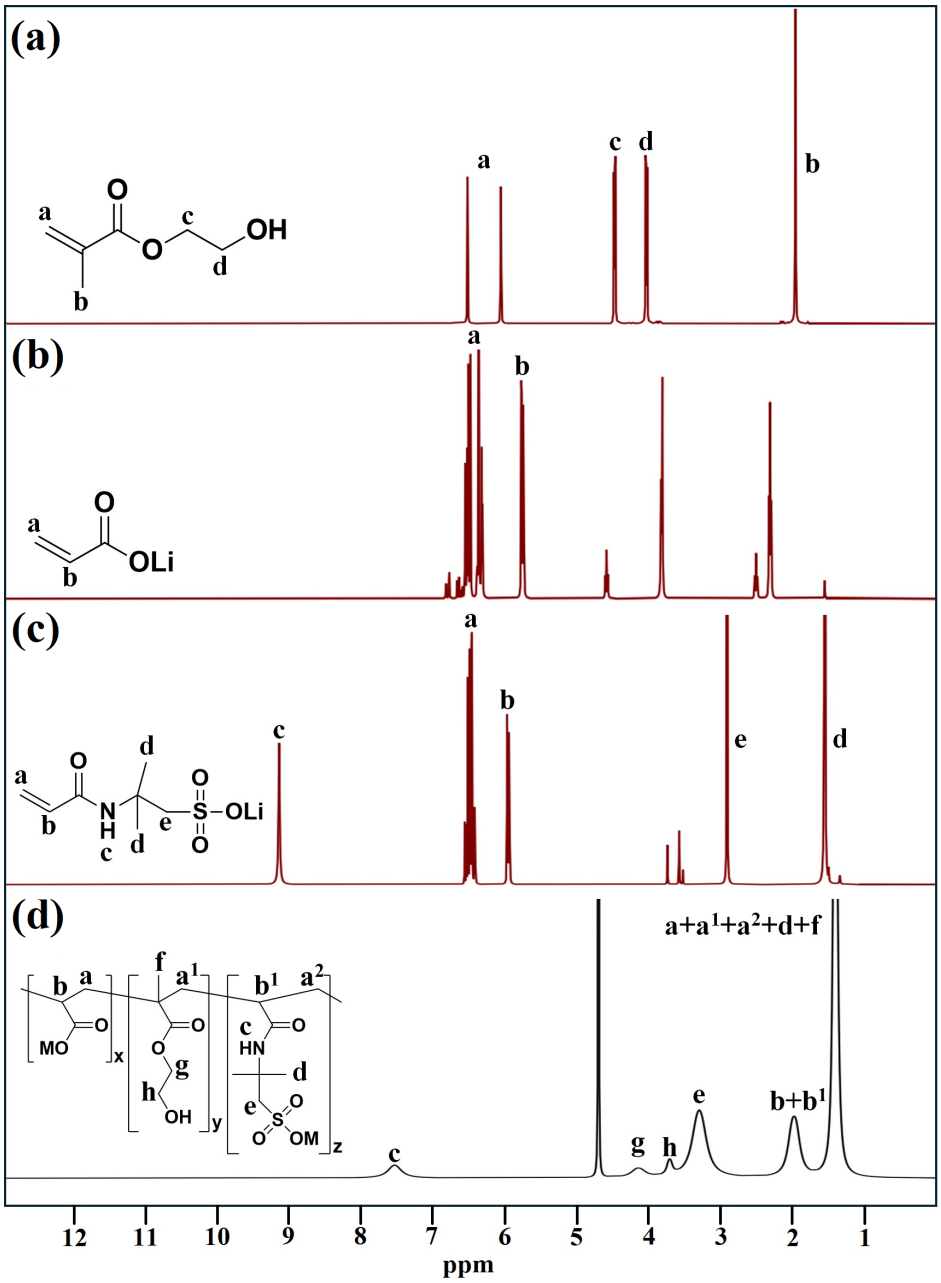

Figure 1. ^{1}H NMR spectrum of (**a**) HEMA, (**b**) LiAA, (**c**) LiAMPS and (**d**) poly (LiAA–HEMA–LiAMPS).

Figure 2 shows the FT–IR spectra of HEMA, LiAA, LiAMPS, and poly (LiAA–HEMA–LiAMPS) to confirm the synthesis of the terpolymer. In Figure 2b,c, the OH peaks of LiAA and LiAMPS around 3350 cm^{-1} indicate the presence of water due to the salt state. The C–H stretching vibrations are observed in the range of 2930–2982 cm^{-1}. In Figure 2d, the stretching vibration absorption peak of the amide group (–CONH–) is at 3335 cm^{-1}. The asymmetric C–H stretching vibrations in methyl (–CH_3) are observed in the range of 2930–2982 cm^{-1}. The amide groups in AMPS are influenced by hydrogen bonding, with the amide C=O stretching (–$CONH_2$–) peak at 1650 cm^{-1}, and NH bending and CN stretching peaks at 1552 cm^{-1}. The symmetric and asymmetric stretching vibrations of the sulfonic acid groups are observed at 1211 cm^{-1} and 1034 cm^{-1}, respectively [45–47]. The carbonyl (C=O) stretching peak in LiAA and HEMA is confirmed at 1715 cm^{-1}. These results indicate that poly (LiAA–HEMA–LiAMPS) has organic functional groups of AA, HEMA, and AMPS.

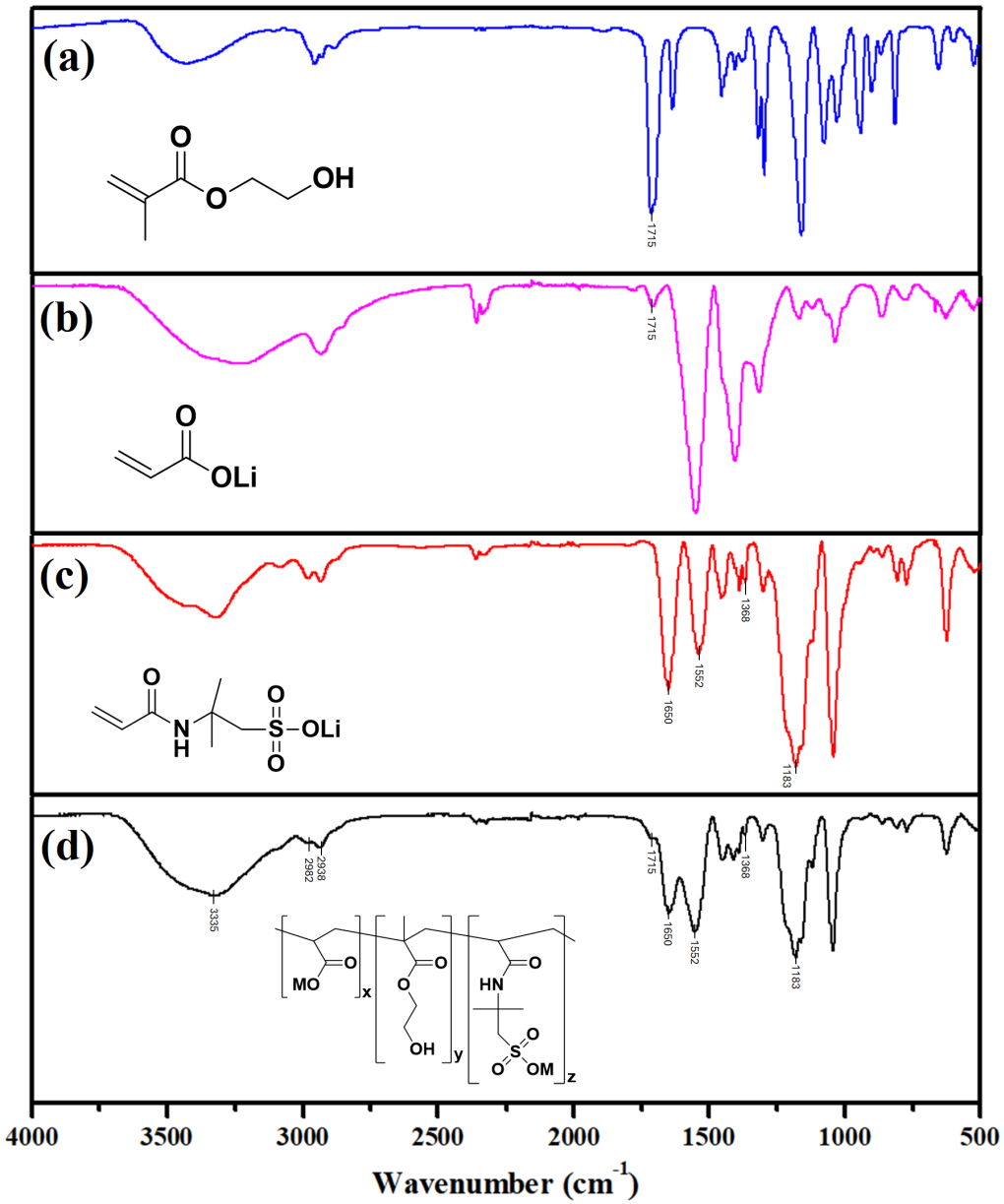

Figure 2. FT-IR spectrum of (**a**) HEMA, (**b**) LiAA, (**c**) LiAMPS and (**d**) poly (LiAA-HEMA-LiAMPS).

Figure 3 shows the tapping mode AFM micrographs of the synthesized BTPE–37 and the PAA–PVA film. Figure 3a,d are at a 50 × 50 magnification, Figure 3b,e are at 20 × 20, and Figure 3c,f are 3D images of Figure 3a,d. The PAA–PVA film (Figure 3d–f) has a generally smooth surface with needle–like lumps formed during drying, similar to other PVA and PAA films [45,46]. BTPE–37 (Figure 3a–c), made with Li–substituted AA and AMPS, shows large and small hemispherical shapes due to the micelle formation from hydrophilic ($–COO^-Li^+$, $–SO_3^-Li^+$) terminal groups of LiAA and LiAMPS and the hydrophobic groups of the polymer backbone [47,48]. This micelle structure enhances Li ion mobility, improving ionic conductivity.

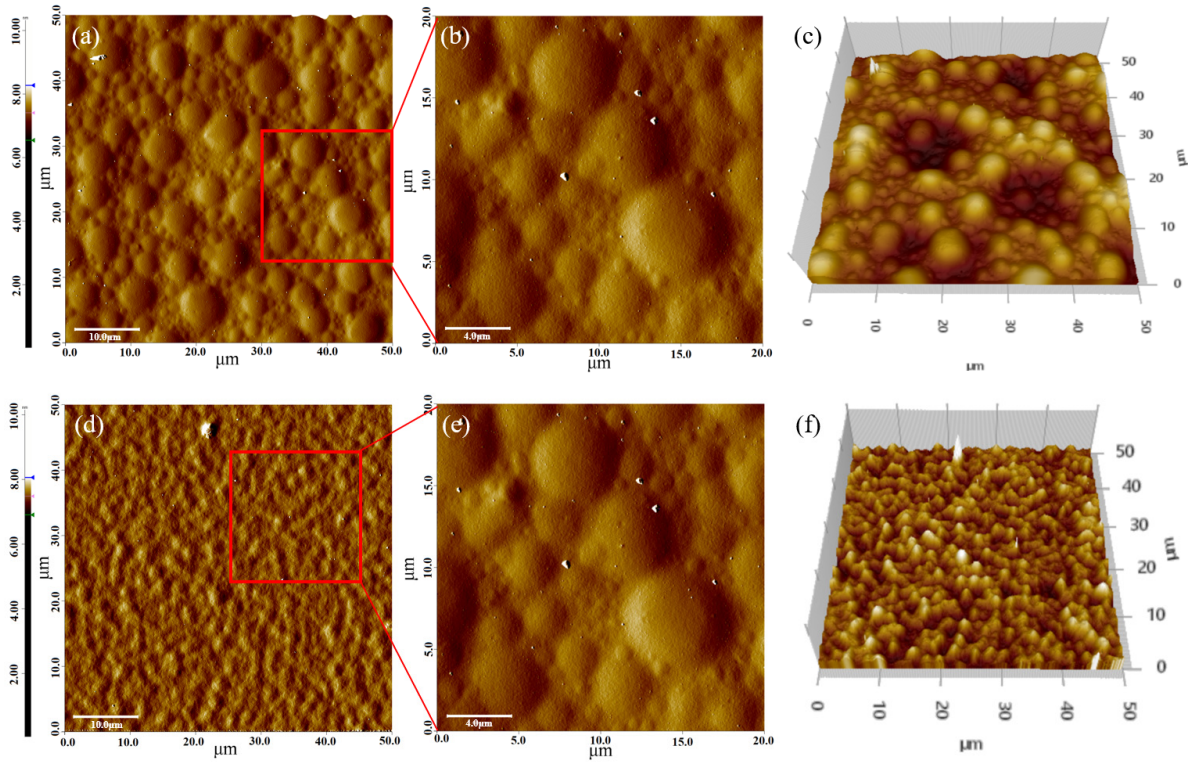

Figure 3. AFM image of BTPE–37 (**a**–**c**) and PAA–PVA (**d**–**f**): (**a**) 2D image of BTPE–37 (50 × 50 μm^2), (**b**) 2D Image of BTPE-37 in the range indicated by the red box in (**a**) (20 × 20 μm^2), (**c**) 3D image of BTPE–37 (50 × 50 μm^2), (**d**) 2D image of PAA–PVA film (50 × 50 μm^2), (**e**) 2D Image of PAA-PVA in the range indicated by the red box in (**d**) (20 × 20 μm^2) and (**f**) 3D image of PAA–PVA film (50 × 50 μm^2).

3.2. Thermal Properties of Blend Terpolymer Electrolyte Membrane

Glass transition (T_g) temperatures of BTPE and terpolymer were measured via DSC in the range of −55 to 40 °C. Figure 4a shows that the T_g of terpolymer, BTPE–010, BTPE–19, BTPE–28, and BTPE–37 are −38.52, −39.96, −40.07, −40.17, and −40.99 °C, respectively. The low T_g indicates excellent chain flexibility in the polymer electrolyte, facilitating smooth lithium-ion movement and high ionic conductivity.

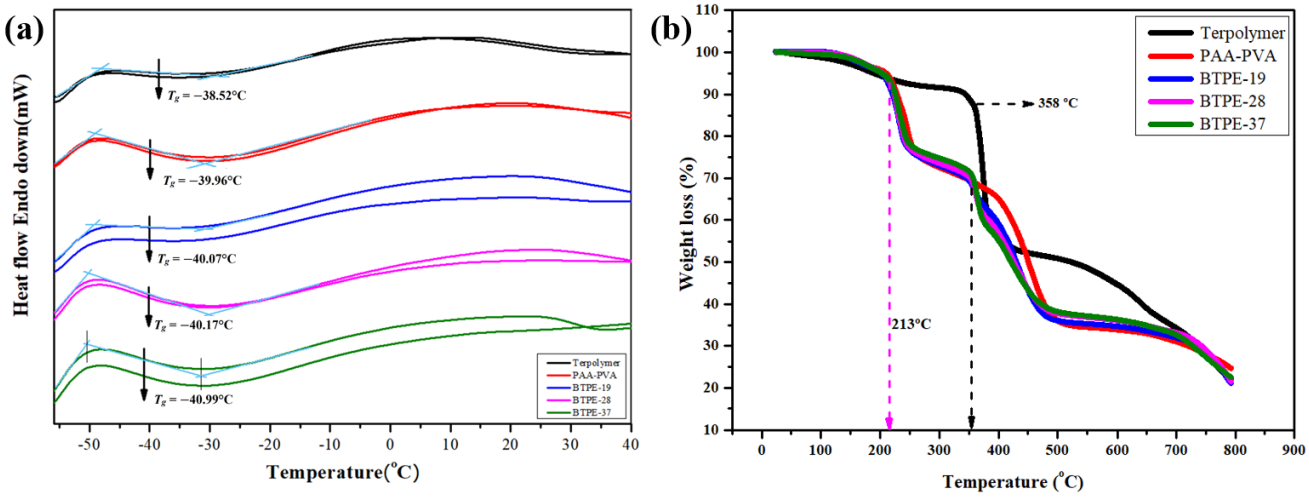

Figure 4. DSC curves (**a**) and TGA curves (**b**) of BTPEs, pure terpolymer, and PAA–PVA.

Figure 4b represents the thermogravimetric analysis (TGA) data of terpolymer and BTPEs in the temperature range of 25 to 800 °C. The terpolymer shows an initial mass loss of about 9.8% up to around 350 °C, due to the physical water absorption. A sharp weight loss of about 36 wt% occurs from 350 to 410 °C, likely due to the decomposition of the precursor and the terpolymer. For BTPE–010, 19, 28, and 37, an initial mass loss of about 6% is observed up to around 210 °C, also due to the water absorption. Subsequently, a sharp mass loss of about 17 wt% occurs from 210 to 260 °C, followed by a second mass loss of about 31 wt% from 350 to 500 °C. These results imply that the blended terpolymer electrolyte membrane provides thermal stability suitable for the operating range of Li–ion batteries.

3.3. Electrochemical Properties of Blended Terpolymer Electrolyte Membrane

The temperature-dependent ionic conductivities of BTPE doped with 2 M LiFSI were calculated using EIS measurements in the range of 30 to 80 °C, as shown in Figure 5 (originating from Figure S2a–d of the Supplementary Information). The ionic conductivities of BTPE–010, BTPE–19, BTPE–28, and BTPE–37 were 1.78, 1.95, 3.11, and 5.21 × 10^{-4} S cm^{-1} at 30 °C; and 3.63, 3.25, 4.52, and 8.11 × 10^{-4} S cm^{-1} at 80 °C, respectively. Higher terpolymer ratios in BTPE–010, 19, 28, and 37 result in increased ionic conductivity due to micellar structures formed by the $O^{-}Li^{+}$ of AA and the $SO_3^{-}Li^{+}$ of AMPS. Additionally, the ionic conductivities of BTPE–010, 19, 28, and 37 with the 1 M LiFSI addition were also measured, showing lower conductivity at low temperatures, and generally unstable plots (Figures S3 and S4).

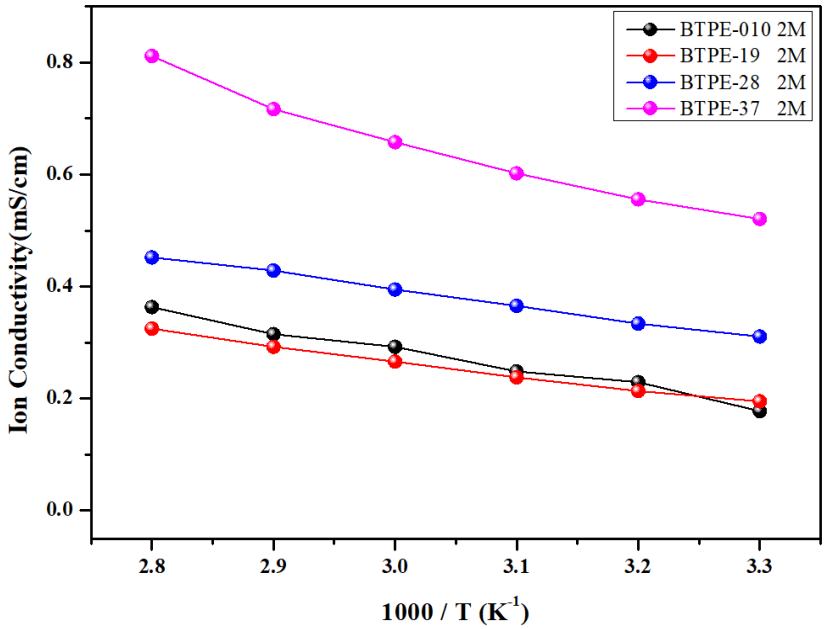

Figure 5. Temperature-dependent ionic conductivity of BTPEs from 30 to 80 °C.

Figure 6 illustrates the electrochemically stable window of BTPE–37 via linear sweep voltammetry (LSV) in the range of –1.5 to 6 V. BTPE–37 demonstrated an anodic stability of about 4.77 V vs. Li/Li^{+}. These findings suggest that BTPE–37 is suitable for the voltage requirement of LFP–based lithium–ion batteries (2.5–4.2 V).

Figure 7 presents the cyclic voltammogram of the $LiFePO_4$/BTPE–37/Li metal battery. The redox peaks were observed at approximately 2.8 V and 5.15 V vs. Li/Li^{+}. Additionally, peaks associated with reversible lithium plating and stripping from the working electrode were observed in the range of about −0.5 to 0.5 V vs. Li/Li^{+}. Minor peaks in the potential

range of 1 to 3 V are likely due to the decomposition of impurities in some reagents (used without post-treatment) or the formation of a solid electrolyte interface (SEI).

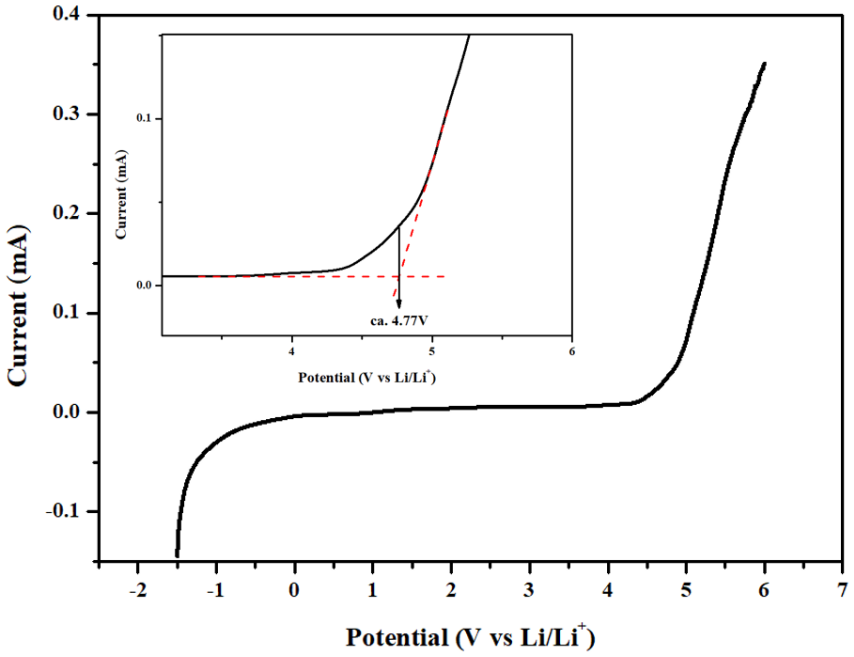

Figure 6. Linear sweep voltammetry (LSV) profiles of BTPE–37.

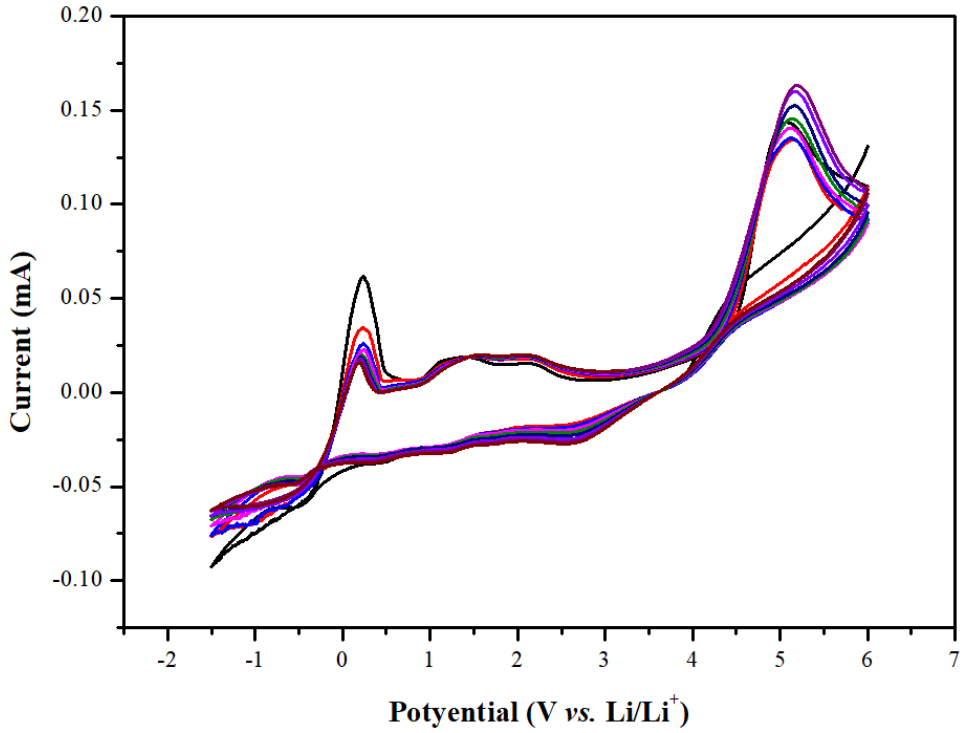

Figure 7. CV profiles of BTPE-37.

Figure 8 presents the lithium-ion transference number (t_+) results obtained via chronoamperometry (CA) and EIS taken before and after CA. The polarization current initially drops and stabilizes within 5000 s. The lithium-ion transference number of the BTPE–37 is calculated to be 0.47. This relatively higher t_+ value, compared to other BTPE ratios, is attributed to the improved lithium transport pathway formed by appropriately increasing the amounts of LiAA and LiAMPS. The t_+ data for BTPE electrolytes with different ratios are shown in Table S3 and Figure S7.

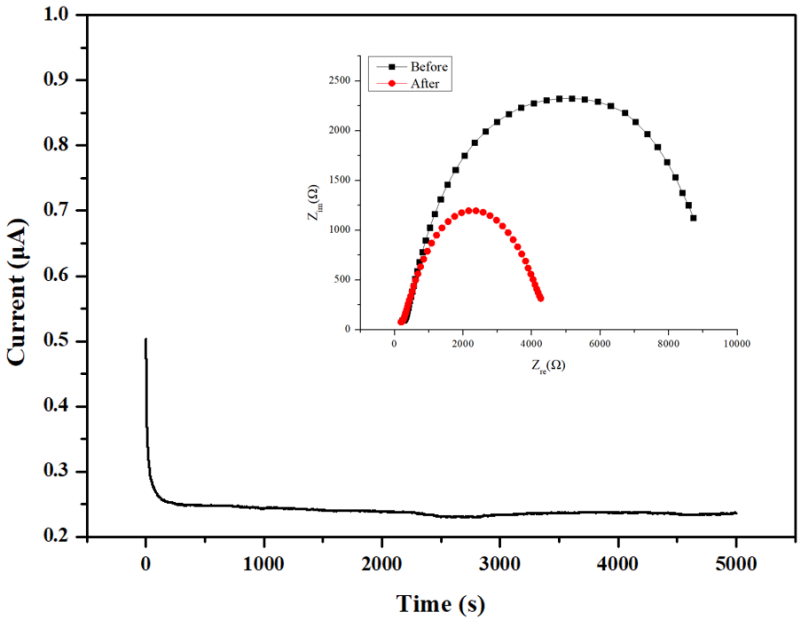

Figure 8. Li transference number (t_+) of BTPE–37.

3.4. Electrochemical Performance of Blended Terpolymer Electrolyte-Based Li Metal Battery

LFP, with a theoretical capacity of 150 mAh g^{-1}, was utilized as a cathode active material due to its excellent cycling performance and tolerance to overcharge. Figure 9 shows the rate performance of the LFP/Li metal battery using BTPE–37 as an electrolyte at different current densities (0.1 to 1 C). The C–rate is based on the theoretical capacity of LFP (1 C—150 mAh g^{-1}). The LFP/BTPE–37/Li cell exhibits average capacities of 136.81, 118.77, 112.04, 101.87, and 130.55 mAh g^{-1} at 0.1, 0.2, 0.5, 1, and 0.1 C, respectively. After increasing the current density and returning to 0.1 C, the discharge capacity decreased by approximately 4.5% from 136.81 mAh g^{-1} to 130.55 mAh g^{-1}.

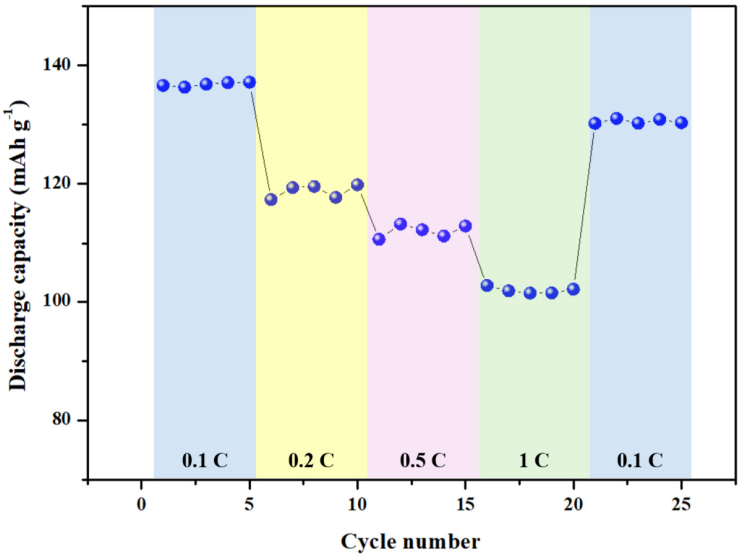

Figure 9. Rate capability of LFP/BTPE–37/Li metal battery.

Figure 10a shows the charge–discharge curves of LFP/Li metal batteries using BTPE–37 as the electrolyte at different cycles at 0.1 C. The first cycle exhibits high voltage flatness which decreases with subsequent cycles. Figure 10b illustrates the cycle stability of LFP/Li metal batteries using BTPE–37 as the electrolyte, measured in the potential range of 2.5 to 3.8 V at 0.1 C for 100 cycles. The initial discharge capacity of the cell was 131.91 mAh

g^{-1}, which decreased by approximately 23.97% to 100.29 mAh g^{-1} after 100 cycles. This capacity decline is due to the fact that the large amount of hydroxyl groups (−OH) in BTPE adsorb moisture, which reacts with LiFSI and the electrode during the charge–discharge process, thereby lowering electrochemical stability and promoting aluminum corrosion, which is an inherent drawback of LiFSI [49,50]. The Coulombic efficiency (η) of the cell based on the BTPE–37 electrolyte was 96.56% in the initial cycle, and slightly increased to 98.55% after 100 cycles, with an average Coulombic efficiency (η) of 97.9%. The increase in Coulombic efficiency with charge–discharge cycling is likely due to the formation of a solid electrolyte interface (SEI) layer on the lithium anode by the LiFSI–based electrolyte, stabilizing the electrolyte interface.

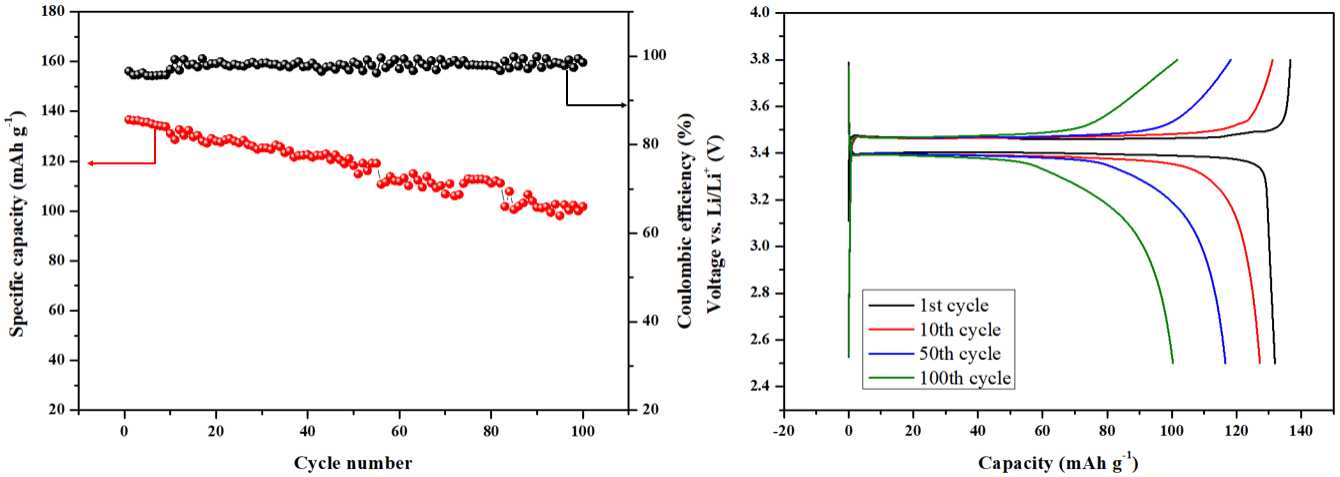

Figure 10. Electrochemical performance of LFP/BTPE–37/Li battery: (**a**) typical charge–discharge voltage profiles of BTPE–37-based battery, (**b**) variants of specific capacity and the coulombic efficiency plot.

4. Conclusions

In this study, we designed a blended terpolymer electrolyte membrane (BTPE) that combines the advantages of SICPE and DICPE to address the safety issue of the existing organic liquid electrolytes of lithium-ion batteries (LIB). BTPE, synthesized from LiAA, LiAMPS, and HEMA-based terpolymer, blended with PAA–PVA, and incorporating LiFSI, exhibited low T_g and high thermal stability, a high lithium transference number (t_+ = 0.47) and ionic conductivity (5.21 × 10^{-4} S cm^{-1} at 30 °C). Additionally, it demonstrated 97.9% coulombic efficiency after 100 cycles. These results suggest that the complementary approach of SICPE and DICPE can enhance the performance and safety of lithium-ion batteries.

Supplementary Materials: The following supporting information can be downloaded at: https://www.mdpi.com/article/10.3390/batteries11030103/s1, Figure S1. Blend terpolymer electrolyte membrane according to different ratio of poly (LiAA-HEMA-LiAMPS) and PAA-PVA; Figure S2. EIS plots of BTPEs with 2M of LiFSI between 30 to 80 °C (a) BTPE-010, (b) BTPE-19, (c) BTPE-28 and (d) BTPE-37; Figure S3. EIS plots of BTPEs with 1M of LiFSI between 30 to 80 °C (a) BTPE-010, (b) BTPE-19, (c) BTPE-28 and (d) BTPE-37; Figure S4. Temperature-dependent ionic conductivity of BTPEs with 1M and 2M of LiFSI in the range of 30 to 80 °C; Figure S5. linear sweep voltammetry plot of BTPE-010(black), BTPE-19(red), BTPE-28(blue) and BTPE-37(pink); Figure S6. Cyclic voltammetry plot of (a) BTPE-010, (b) BTPE-19 and (c) BTPE-28; Figure S7. Lithium transference number plot of (a) BTPE-010, (b) BTPE-19 and (c) BTPE-28; Table S1. The manufacturing ratio of Blend terpolymer

electrolyte; Table S2. The manufacturing ratio of Blend terpolymer electrolyte different LiFSI amount for EIS; Table S3. Currents and resistances of the electrolytes for t_+ calculation.

Author Contributions: Experiments, material synthesis, data result analysis, writing—original draft, and methodology, W.B.; data result analysis, K.J., S.S., D.K., H.N. and D.L.; data curation, J.L.; conceptualization and writing—review & editing, S.C.S. and W.K.; supervision, data curation, and editing, H.J. All authors have read and agreed to the published version of the manuscript.

Funding: This research received no external funding.

Data Availability Statement: The data presented in this study are available on request from the corresponding author.

Acknowledgments: This paper was supported by Konkuk University in 2023.

Conflicts of Interest: The authors declare no competing financial interests or personal relationships that could influence the work reported in this study.

References

1. Liu, K.; Liu, Y.; Lin, D.; Pei, A.; Cui, Y. Materials for Lithium-Ion Battery Safety. *Sci. Adv.* **2018**, *4*, eaas9820. [CrossRef] [PubMed]
2. Nair, J.R.; Imholt, L.; Brunklaus, G.; Winter, M. Lithium Metal Polymer Electrolyte Batteries: Opportunities and Challenges. *Electrochem. Soc. Interface* **2019**, *28*, 55. [CrossRef]
3. Liu, W.; Placke, T.; Chau, K.T. Overview of Batteries and Battery Management for Electric Vehicles. *Energy Rep.* **2022**, *8*, 4058–4084. [CrossRef]
4. Fan, X.; Wang, C. High-Voltage Liquid Electrolytes for Li Batteries: Progress and Perspectives. *Chem. Soc. Rev.* **2021**, *50*, 10486–10566. [CrossRef] [PubMed]
5. Pullanchiyodan, A.; Joy, R.; Sreeram, P.; Raphael, L.R.; Das, A.; Balakrishnan, N.T.M.; Ahn, J.-H.; Vlad, A.; Sreejith, S.; Raghavan, P. Recent Advances in Electrospun Fibers Based on Transition Metal Oxides for Supercapacitor Applications: A Review. *Energy Adv.* **2023**, *2*, 922–947. [CrossRef]
6. Zu, C.; Yu, H.; Li, H. Enabling the Thermal Stability of Solid Electrolyte Interphase in Li-ion Battery. *InfoMat* **2021**, *3*, 648–661. [CrossRef]
7. Balakrishnan, N.T.M.; Das, A.; Joyner, J.D.; Jabeen Fatima, M.J.; Raphael, L.R.; Pullanchiyodan, A.; Raghavan, P. Quest for High-Performance Gel Polymer Electrolyte by Enhancing the Miscibility of the Bi-Polymer Blend for Lithium-Ion Batteries: Performance Evaluation in Extreme Temperatures. *Mater. Today Chem.* **2023**, *29*, 101407. [CrossRef]
8. Zhao, N.; Khokhar, W.; Bi, Z.; Shi, C.; Guo, X.; Fan, L.-Z.; Nan, C.-W. Solid Garnet Batteries. *Joule* **2019**, *3*, 1190–1199. [CrossRef]
9. Wang, L.P.; Zhang, X.D.; Wang, T.S.; Yin, Y.X.; Shi, J.L.; Wang, C.R.; Guo, Y.G. Ameliorating the Interfacial Problems of Cathode and Solid-State Electrolytes by Interface Modification of Functional Polymers. *Adv. Energy Mater.* **2018**, *8*, 1801528. [CrossRef]
10. Reinoso, D.M.; Frechero, M.A. Strategies for Rational Design of Polymer-Based Solid Electrolytes for Advanced Lithium Energy Storage Applications. *Energy Storage Mater.* **2022**, *52*, 430–464. [CrossRef]
11. Zhou, T.; Shi, D.; Wang, Q.; Yang, C.; Wang, X.; Wu, K.; Mu, Y.; Wu, J.; Liu, Z.; Liu, W. Accelerating Li+/Li Redox through the Regulation of the Electric Double Layer for Efficient Lithium Metal Anodes. *Chem. Eng. J.* **2023**, *468*, 143676. [CrossRef]
12. Liu, Y.; Li, Y.; Du, Z.; He, C.; Bi, J.; Li, S.; Guan, W.; Du, H.; Ai, W. Integrated Gradient Cu Current Collector Enables Bottom-Up Li Growth for Li Metal Anodes: Role of Interfacial Structure. *Adv. Sci.* **2023**, *10*, 2301288. [CrossRef] [PubMed]
13. Hua, W.; Dandan, Y.; Chengwei, K.; Liwei, C.; Wang, L.; Xilan, F.; Zheng, Z.; Xinbo, Z.; Yu, Z. Alkali Metal Anodes for Rechargeable Batteries. *Chem* **2019**, *5*, 313–338.
14. Dai, H.; Xi, K.; Liu, X.; Lai, C.; Zhang, S. Cationic Surfactant-Based Electrolyte Additives for Uniform Lithium Deposition via Lithiophobic Repulsion Mechanisms. *J. Am. Chem. Soc.* **2018**, *140*, 17515–17521. [CrossRef]
15. Zhang, H.; Eshetu, G.G.; Judez, X.; Li, C.; Rodriguez-Martínez, L.M.; Armand, M. Electrolyte Additives for Lithium Metal Anodes and Rechargeable Lithium Metal Batteries: Progress and Perspectives. *Angew. Chem. Int. Ed.* **2018**, *57*, 15002–15027. [CrossRef]
16. Zhou, T.; Mu, Y.; Chen, L.; Li, D.; Liu, W.; Yang, C.; Zhang, S.; Wang, Q.; Jiang, P.; Ge, G.; et al. Toward Stable Zinc Aqueous Rechargeable Batteries by Anode Morphology Modulation via Polyaspartic Acid Additive. *Energy Storage Mater.* **2022**, *45*, 777–785. [CrossRef]
17. Li, M.; Wang, C.; Chen, Z.; Xu, K.; Lu, J. New Concepts in Electrolytes. *Chem. Rev.* **2020**, *120*, 6783–6819. [CrossRef] [PubMed]
18. Hatzell, K.B.; Chen, X.C.; Cobb, C.L.; Dasgupta, N.P.; Dixit, M.B.; Marbella, L.E.; McDowell, M.T.; Mukherjee, P.P.; Verma, A.; Viswanathan, V. Challenges in Lithium Metal Anodes for Solid-State Batteries. *ACS Energy Lett.* **2020**, *5*, 922–934. [CrossRef]
19. Wang, Q.; Wang, H.; Wu, J.; Zhou, M.; Liu, W.; Zhou, H. Advanced Electrolyte Design for Stable Lithium Metal Anode: From Liquid to Solid. *Nano Energy* **2021**, *80*, 105516. [CrossRef]

20. Li, Z.; Lu, W.; Zhang, N.; Pan, Q.; Chen, Y.; Xu, G.; Zeng, D.; Zhang, Y.; Cai, W.; Yang, M. Single Ion Conducting Lithium Sulfur Polymer Batteries with Improved Safety and Stability. *J. Mater. Chem. A Mater.* **2018**, *6*, 14330–14338. [CrossRef]
21. Quartarone, E.; Mustarelli, P.; Magistris, A. PEO-Based Composite Polymer Electrolytes. *Solid State Ion.* **1998**, *110*, 1–14. [CrossRef]
22. Tarascon, J.-M.; Armand, M. Issues and Challenges Facing Rechargeable Lithium Batteries. *Nature* **2001**, *414*, 359–367. [CrossRef] [PubMed]
23. Xi, C.; Cui, X.; Zhang, R.; Guo, J.; Li, R.; Chao, Y.; Xu, G.; He, C.; Chen, F.; Li, L.; et al. Utilizing an Oxygen-Rich Interface by Hydroxyapatite to Regulate the Linear Diffusion for the Stable Solid-State Electrolytes. *ACS Appl. Mater. Interfaces* **2022**, *14*, 33392–33399. [CrossRef] [PubMed]
24. Deng, R.; Ke, B.; Xie, Y.; Cheng, S.; Zhang, C.; Zhang, H.; Lu, B.; Wang, X. All-Solid-State Thin-Film Lithium-Sulfur Batteries. *Nanomicro Lett.* **2023**, *15*, 73. [CrossRef]
25. Long, L.; Wang, S.; Xiao, M.; Meng, Y. Polymer Electrolytes for Lithium Polymer Batteries. *J. Mater. Chem. A Mater.* **2016**, *4*, 10038–10069. [CrossRef]
26. Jin, L.; Lim, H.; Bae, W.; Song, S.; Joo, K.; Jang, H.; Kim, W. Crosslinked Gel Polymer Electrolyte from Trimethylolpropane Triglycidyl Ether by In Situ Polymerization for Lithium-Ion Batteries. *Gels* **2024**, *10*, 40. [CrossRef]
27. Zhang, W.; Jin, L.; Bae, W.; Park, S.; Jeon, M.; Lee, S.; Lee, S.; Jang, H.; Kim, W. In-Situ Generated Solid-State Electrolytes with Intimate Interface Affinity Enable Conductivity and High Performances for Lithium-Ion Batteries. *Electrochim. Acta* **2023**, *465*, 142932. [CrossRef]
28. Grewal, M.S.; Tanaka, M.; Kawakami, H. Bifunctional Poly(Ethylene Glycol) Based Crosslinked Network Polymers as Electrolytes for All-Solid-State Lithium Ion Batteries. *Polym. Int.* **2019**, *68*, 684–693. [CrossRef]
29. Ma, Y.; Sun, Q.; Wang, S.; Zhou, Y.; Song, D.; Zhang, H.; Shi, X.; Zhang, L. Li Salt Initiated In-Situ Polymerized Solid Polymer Electrolyte: New Insights via in-Situ Electrochemical Impedance Spectroscopy. *Chem. Eng. J.* **2022**, *429*, 132483. [CrossRef]
30. Baik, J.H.; Kim, S.; Hong, D.G.; Lee, J.C. Gel Polymer Electrolytes Based on Polymerizable Lithium Salt and Poly(Ethylene Glycol) for Lithium Battery Applications. *ACS Appl. Mater. Interfaces* **2019**, *11*, 29718–29724. [CrossRef]
31. Guo, J.; Chen, Y.; Xiao, Y.; Xi, C.; Xu, G.; Li, B.; Yang, C.; Yu, Y. Flame-Retardant Composite Gel Polymer Electrolyte with a Dual Acceleration Conduction Mechanism for Lithium Ion Batteries. *Chem. Eng. J.* **2021**, *422*, 130526. [CrossRef]
32. Chen, L.; Li, W.; Fan, L.; Nan, C.; Zhang, Q. Intercalated Electrolyte with High Transference Number for Dendrite-free Solid-state Lithium Batteries. *Adv. Funct. Mater.* **2019**, *29*, 1901047. [CrossRef]
33. Maia, B.A.; Magalhães, N.; Cunha, E.; Braga, M.H.; Santos, R.M.; Correia, N. Designing Versatile Polymers for Lithium-Ion Battery Applications: A Review. *Polymers* **2022**, *14*, 403. [CrossRef] [PubMed]
34. Li, H.; Du, Y.; Zhang, Q.; Zhao, Y.; Lian, F. A Single-ion Conducting Network as Rationally Coordinating Polymer Electrolyte for Solid-state Li Metal Batteries. *Adv. Energy Mater.* **2022**, *12*, 2103530. [CrossRef]
35. Liew, C.-W.; Ng, H.M.; Numan, A.; Ramesh, S. Poly(Acrylic Acid)–Based Hybrid Inorganic–Organic Electrolytes Membrane for Electrical Double Layer Capacitors Application. *Polymers* **2016**, *8*, 179. [CrossRef]
36. Wang, L.; Huang, J.; Shen, Y.; Ma, M.; Ruan, W.; Zhang, M. ARGET-ATRP-Mediated Grafting of Bifunctional Polymers onto Silica Nanoparticles Fillers for Boosting the Performance of High-Capacity All-Solid-State Lithium–Sulfur Batteries with Polymer Solid Electrolytes. *Polymers* **2024**, *16*, 1128. [CrossRef]
37. Hu, T.; Shen, X.; Peng, L.; Liu, Y.; Wang, X.; Ma, H.; Zhang, P.; Zhao, J. Preparation of Single-Ion Conductor Solid Polymer Electrolyte by Multi-Nozzle Electrospinning Process for Lithium-Ion Batteries. *J. Phys. Chem. Solids* **2021**, *158*, 110229. [CrossRef]
38. Gao, J.; Wang, C.; Han, D.W.; Shin, D.M. Single-Ion Conducting Polymer Electrolytes as a Key Jigsaw Piece for next-Generation Battery Applications. *Chem. Sci.* **2021**, *12*, 13248–13272. [CrossRef]
39. Abu-Saied, M.A.; El Desouky, E.A.; Rafea, M.A.; Abusaif, M.S. Toward Highly Ionic Polyelectrolyte Membrane: Synthesis, Characterization, Membrane Performance and Theoretical Studies of PVDF-g-PAN/PAMPS Hybrid Membranes. *Mater. Today Commun.* **2024**, *40*, 110232. [CrossRef]
40. Lee, A.-R.; Kim, Y.-D.; Lee, S.-K.; Jo, N.-J. Poly (Hydroxyethyl Methacrylate) Based Networked Solid Polymer Electrolyte. *J. Nanosci. Nanotechnol.* **2013**, *13*, 7208–7211. [CrossRef]
41. Wu, G.M.; Lin, S.J.; Yang, C.C. Preparation and Characterization of PVA/PAA Membranes for Solid Polymer Electrolytes. *J. Memb. Sci.* **2006**, *275*, 127–133. [CrossRef]
42. Thayumanasundaram, S.; Rangasamy, V.S.; Seo, J.W.; Locquet, J.-P. Electrochemical Performance of Polymer Electrolytes Based on Poly(Vinyl Alcohol)/Poly(Acrylic Acid) Blend and Pyrrolidinium Ionic Liquid for Lithium Rechargeable Batteries. *Electrochim. Acta* **2017**, *240*, 371–378. [CrossRef]
43. Ni, H.; Yang, Y.; Chen, Y.; Liu, J.; Zhang, L.; Wu, M. Preparation of a Poly(DMAEMA-Co-HEMA) Self-Supporting Microfiltration Membrane with High Anionic Permselectivity by Electrospinning. *e-Polymers* **2017**, *17*, 149–157. [CrossRef]
44. Abdiyev, K.Z.; Maric, M.; Orynbayev, B.Y.; Toktarbay, Z.; Zhursumbaeva, M.B.; Seitkaliyeva, N.Z. Flocculating Properties of 2-Acrylamido-2-Methyl-1-Propane Sulfonic Acid-Co-Allylamine Polyampholytic Copolymers. *Polym. Bull.* **2022**, *79*, 10741–10756. [CrossRef]

45. Rattanawongwiboon, T.; Ghaffarlou, M.; Sütekin, S.D.; Pasanphan, W.; Güven, O. Preparation of Multifunctional Poly (Acrylic Acid)-Poly (Ethylene Oxide) Nanogels from Their Interpolymer Complexes by Radiation-Induced Intramolecular Crosslinking. *Colloid. Polym. Sci.* **2018**, *296*, 1599–1608. [CrossRef]
46. Mehto, A.; Mehto, V.R.; Chauhan, J. Preparation and Characterization of Polyvinyl Alcohol (PVA)/ZrO_2 Composite Membranes. *Phys. Status Solidi (B)* **2023**, *260*, 2300164. [CrossRef]
47. Yan, X.; Xu, Z.; Yuan, S.; Han, A.; Shen, Y.; Cheng, X.; Liang, Y.; Shen, S.; Zhang, J. Structural and Transport Properties of Ultrathin Perfluorosulfonic Acid Ionomer Film in Proton Exchange Membrane Fuel Cell Catalyst Layer: Ass Review. *J. Power Sources* **2022**, *536*, 231523. [CrossRef]
48. Wang, Y.; Pang, Y.; Xu, H.; Martinez, A.; Chen, K.S. PEM Fuel Cell and Electrolysis Cell Technologies and Hydrogen Infrastructure Development—A Review. *Energy Environ. Sci.* **2022**, *15*, 2288–2328. [CrossRef]
49. Daojun, Y.; Xiaojie, L.; Ningning, W.; Wenhuai, T. Effect of moisture content on the electrochemical performance of $LiNi_{1/3}Co_{1/3}Mn_{1/3}O_2$/graphite battery. *Electrochim. Acta* **2016**, *188*, 611–618.
50. Guochun, Y.; Xinhai, L.; Zhixing, W.; Huajun, G.; Wenjie, P.; Qiyang, H. Lithium difluoro(oxalato)borate as an additive to suppress the aluminum corrosion in lithium bis(fluorosulfonyl)imide-based nonaqueous carbonate electrolyte. *J. Solid. State Electrochem.* **2016**, *20*, 507–516.